

Characterizing Boosted Dijet Resonances with Jet Energy Correlators

R. Sekhar Chivukula,¹ Kirtimaan A. Mohan,¹
 Dipan Sengupta,¹ and Elizabeth H. Simmons^{1,2}

¹ *Department of Physics and Astronomy Michigan State University, East Lansing, MI, U.S.A.*

² *University of California San Diego, La Jolla, CA, U.S.A.*

We show that Jet Energy Correlation variables can be used effectively to discover and distinguish a wide variety of boosted light dijet resonances at the LHC through sensitivity to their transverse momentum and color structures.

The LHC is actively seeking dijet resonances. However, for a given resonance mass, the ability to probe smaller couplings to quarks and gluons depends on the amount of data collected and how well one can reduce Standard Model (SM) backgrounds. Sensitivity to light dijet resonances at the LHC, in particular, is limited by the presence of large SM backgrounds that accumulate at a rate which is difficult to manage by currently available trigger and data acquisition systems at ATLAS and CMS. Looking for such resonances produced with high transverse momenta in association with a jet, photon, W^\pm or Z boson (or even in pair production of the resonances) can reduce both signal and background rates thus avoiding trigger threshold limitations. Additionally, for highly boosted light resonances, jet substructure techniques can be applied to further reduce backgrounds.

Recently, using this search strategy, ATLAS [1] and CMS [2] were able to set limits on narrow light vector resonances (specifically a leptophobic Z' [3]), decaying to a pair of jets, in a coupling and mass range (100–600) GeV that was not accessible to earlier colliders such as UA2 and CDF. However there are a plethora of possible dijet resonances that could exist: colorons [4], sextet and triplet diquarks [5, 6], excited quarks [7, 8], color-octet scalars [9], massive spin-2 particles [10] to name a few. While substructure techniques can unearth new resonances, once a light resonance is discovered the primary task becomes understanding the nature of the resonance itself. In this note we demonstrate how Jet Energy Correlators (JECs) aid in differentiating between these numerous types of resonances ¹.

New dijet resonances may be classified

¹ Elsewhere we will consider and compare other jet

according to their spin and color structure [16]. While resonances of different spin can be differentiated on the basis of angular distributions of their decay products, identifying types of resonances on the basis of their color structure is more difficult. Note that the color discriminant variable [17, 18] will not be useful for (relatively) weakly-coupled light resonances since their decay widths are too narrow to be measured at the LHC. We exhibit the power of JEC in this regard by examining some benchmark models² listed below:

- A color singlet leptophobic Z' that couples to baryon number via $\frac{g_B}{6} \bar{q} \gamma^\mu q Z'_\mu$ [3].
- A color octet coloron C_μ interacting with quarks through $g_s \tan \theta \bar{q} T^a \gamma^\mu q C_\mu^a$ [4].
- A color sextet diquark (Φ_6^γ) that interacts with pairs of quarks through $\sqrt{2} (\bar{K}_6)^{ab} \lambda_\Phi \Phi_6^\gamma \bar{u}_{Ra}^c u_{Lb}$ [5, 18].
- A color triplet excited quark (q^*) interacting with quarks and gluons (as well as other gauge bosons) through the interaction term $\frac{1}{2\Lambda} \bar{q}_R^* \sigma^{\mu\nu} [g_s f_S \frac{\lambda^a}{2} G_{\mu\nu}^a] q_L$ [8].
- A massive color singlet, spin 2 object ($X^{\mu\nu}$) that interacts with SM particles through the energy momentum tensor $T_{\mu\nu}$ as $\frac{1}{\Lambda} X^{\mu\nu} T_{\mu\nu}$ [10].

observables such as N-Subjetiness [11, 12] and Jet Energy Profiles [13], jet pull [14] and dipolarity [15].

² We restrict ourselves to leptophobic models only.

- A color octet (but electroweak singlet) scalar S_8 that interacts with gluons through the field strength tensor as $\frac{g_s d_{ABC} k_s}{\Lambda} S_8^A G_{\mu\nu}^B G^{C,\mu\nu}$ [9, 19].

While this list is not exhaustive, these examples serve to illustrate the utility of this method.

The signal process of interest is the production of various resonances in association with a jet, viz. $(pp \rightarrow X(\rightarrow jj) + j ; X \in \{Z'_\mu, C_\mu, \Phi_6, q^*, X^{\mu\nu}, S_8\})$ ³, where the resonance is boosted sufficiently that its decay products lie within a single “fat jet”. The dominant background originates from QCD multijet events. The various resonance models were implemented in **FeynRules** [20]. Parton level events for both signal and background were simulated using **MADGRAPH_AMC@NLO** [21] assuming 13 TeV LHC energy, with subsequent showering and hadronization performed using **PYTHIA8** [22]. We use **FASTJET** [23] to reconstruct jets and calculate JECs. Additionally jet energy smearing and detector granularity are simulated using **Delphes3** [24] with parameters similar to ATLAS. We use the Cambridge-Aachen algorithm [25] to construct fat-jets of radius $R = 1.0$ and use the mass-drop tagger [12] to resolve the fat jets into subjets to reconstruct the mass of the resonance X within $M_X \pm 20$ GeV to help reduce the background. Importantly, we find that the mass-drop tagger does not significantly affect JEC distributions of unfiltered signal fat-jets. Further, the acceptance of the tagger

³ We also performed an analogous analysis of the production of the resonances in association with a W boson, which will be reported in a future work.

does not depend significantly on the nature of the resonance. We require $H_T = \Sigma p_T > 900$ GeV and $p_T^{\text{fatjet}} > 500$ GeV. We use MCFM [26] to determine K-factors for NLO production of the $V + \text{jets}$, $t\bar{t}$ and single top backgrounds. NLO K-factors for the dijet production cross-section were determined using POWHEGBOX [27–29]. Further, we use the MLM [30] matching procedure in PYTHIA8 for multi-jet events that were generated in MADGRAPH_AMC@NLO.

For the purpose of demonstration, the mass of the resonance is set to $M_X = 250$ GeV. The current 95 % CL bound on a 250 GeV leptophobic Z' from 35.9 fb^{-1} of 13 TeV data is $g_b \lesssim 1.5$ ($g_q \lesssim 0.22$), compared with an expected bound of $g_b \lesssim 1.1$ [2]. We therefore consider a Z' resonance with $g_b = 0.6$, which is still allowed by the data. For this coupling, we find that the cross section after all cuts is 25 fb. For all other resonances we adjust the value of the couplings such that for all resonances under consideration, the cross-section after cuts is 25 fb. We find that our total background is ~ 50 pb with the dominant contribution coming from QCD multi-jet processes. We find that with our cuts we expect $S/\sqrt{B} \sim 1.9\sigma$ which is comparable to the expectations of experimental results.

JECs were originally introduced in [31, 32] as a two point correlator, and generalized in [33]. Studies on JEC have focused on standard model processes, specially to distinguish quark jets from gluon jets. Additionally, JECs have been shown to be able to differentiate boosted Higgs and top quarks from QCD backgrounds [33].

The N-point generalized JEC is defined as

[33],

$$ECF(N, \beta) = \sum_{(i_1 < \dots < i_N \in J)} \prod_{a=1}^N p_{Ti_a} \left(\prod_{b=1}^{N-1} \prod_{c=b+1}^N R_{i_b i_c} \right)^\beta. \quad (1)$$

The sum runs over all objects (tracks⁴ or calorimeter cells) within a system J (individual jets or all final states of the collision). p_{Ti} is the transverse momentum of each constituent object. The variable $R_{ij} = \sqrt{(\eta_i - \eta_j)^2 + (\theta_i - \theta_j)^2}$, denotes a pairwise distance measure and is raised to the power β . Here η_i is the pseudo-rapidity while θ_i is the azimuthal angle of particle i . The entire function is infrared and collinear safe for $\beta > 0$.

Using Eq. 1 one can construct a dimensionless double ratio as

$$C_N^{(\beta)} = \frac{ECF(N+1, \beta)ECF(N-1, \beta)}{ECF(N, \beta)^2}. \quad (2)$$

In general, $C_N^{(\beta)}$ quantifies radiation of higher order α_s^n , emerging out of leading order hard sub-jets. In a boosted $Z' \rightarrow j_1 j_2$ like system, if $C_2^{(\beta)} < C_1^{(\beta)}$, the fat jet has two resolved hard subjets, and higher order substructure is mostly soft or collinear. With subsequent soft emissions of the final state, one can assume $p_T^{j_1} \simeq p_T^{j_2} \gg p_T^{j_i}$, where $i > 2$. Thus, the leading approximation can be written as,

$$C_1^{(1)} \simeq R_{12}/4. \quad (3)$$

Since $R_{12} \simeq 2m_{Z'}/p_T^j$, $C_1^{(1)}$ is directly related to the boost of the resonance. We show the distribution of $C_1^{(1)}$ for various resonances in Fig. 1. Since we require $R \leq 1.0$

⁴ Here we define the JECs in terms of the individual particles in the “fat jet” in the simulated event, after using the detector simulation as noted above.

and $p_T^{\text{fat-jet}} > 500$ GeV, we see that $C_1^{(1)} \lesssim 0.25$. Further, since the p_T spectrum is almost identical for all resonances under consideration the distribution for $C_1^{(1)}$ look the same. The p_T distribution for q^* and $X^{\mu\nu}$ are slightly harder (and therefore $C_1^{(1)}$ is shifted to smaller values) since their interactions are mediated by dimension 5 operators. We would also like to point out here that information about the initial state and therefore the nature of the resonance can be gleaned by comparing the p_T distribution for cases when the resonance is produced in association with other particles such as a W -boson. The lower end of the $C_1^{(1)}$ distribution is bounded by detector resolution. This is the minimal separation between subjets that can be resolved, and is encoded in our implementation of the mass drop tagger.

Higher point moments of the JEC depend crucially on the nature of the resonance, in particular, the color structure not only of the resonance but also its decay products – in particular, since $C_F < C_A$, a color octet will radiate more widely than a color triplet. This implies that the correlator double ratios $C_N^{(\beta)}$ should in general be larger for a color octet than a color triplet and smallest for a color singlet.

In Fig. 2 we present distributions for the double ratios $C_2^{(2)}$. To understand the behavior of $C_2^{(\beta)}$, consider a simplified scenario of the two body hadronic decay of a resonance X with one soft emission– $X \rightarrow 1 + 2 + 3_{\text{soft}}$ where 3_{soft} originates from 1. We also expect the distance measure R_{13} to be small and $p_T^{j1} \simeq p_T^{j2} (= p_T) \gg p_T^{j3}$ in the soft and collinear approximation . $C_2^{(\beta)}$ can then be

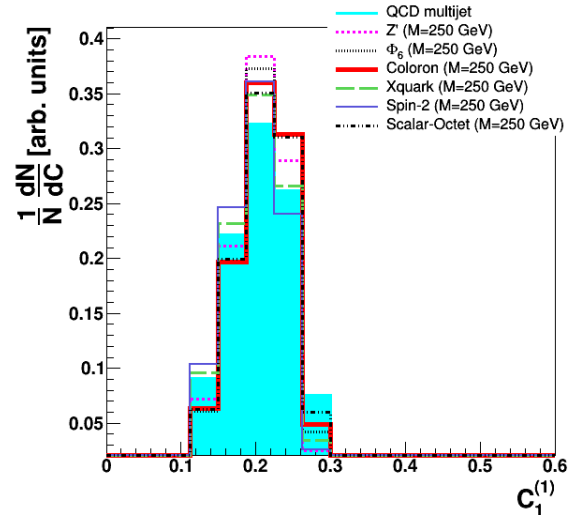


FIG. 1. The double ratio distribution for $C_1^{(1)}$ for the different kinds of resonances under consideration; Z' in pink (small-dashed), sextet-diquark Φ_6 in black (dotted) , Coloron (C_μ) in red (bold,thick), excited quark (q^* , Xquark) in green (large-dashed), Spin-2 ($X^{\mu\nu}$) in blue (bold,thin), scalar color octet (S_8) in black (dot-dashed) . The cyan shaded region corresponds to the distribution of the multi-jet background.

approximated as

$$C_2^{(\beta)} \simeq \frac{2\varepsilon R_{12}^\beta R_{13}^\beta R_{23}^\beta}{(R_{12}^\beta + \varepsilon R_{13}^\beta + \varepsilon R_{23}^\beta)^2} ; \quad (4)$$

note that $\varepsilon R_{13} = (p_T^{j3}/p_T) R_{13} \ll 1$ is doubly suppressed since the third jet, 3_{soft} , is both low-momentum and collinear with jet 1. We therefore expect $C_2^{(2)}$ to peak near 0 as seen in Fig. 2. As discussed earlier, a small $C_2^{(2)}$ implies that the event is mostly a two prong subjet system.

In Fig. 2 we also see, as expected, that the color singlet Z' has the smallest values for $C_2^{(2)}$ whereas, due to the presence of more radiation, the colored objects have larger values. Although the spin-2 is a color singlet its

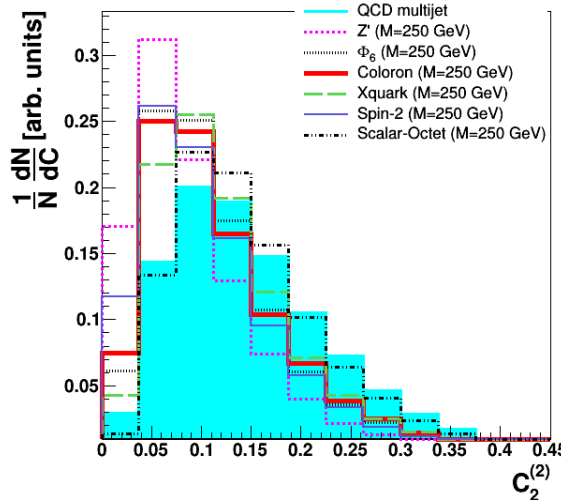


FIG. 2. The double ratio distributions $C_2^{(2)}$ for the resonances and the multi-jet background.

distribution is not identical to Z' and instead has larger values of $C_2^{(2)}$. This is because the spin-2 predominantly decays to gluons, which themselves produce broader jets (since $C_F < C_A$), whereas the coloron and Z' decays to quarks, which produce narrower radiation patterns. As expected, the color octet scalar resonance has the largest values of $C_2^{(2)}$ since it is itself an octet which decays to a pair of octets (gluons). Also shown in Fig. 2 is the distribution of $C_2^{(2)}$ for the dominant multi-jet background. We see that its distribution is significantly different from most of the signal distributions and therefore the JECs can be used not only to discriminate between different signals but also to discriminate signal from background.⁵ The scalar octet behaves most like the QCD multi-jet

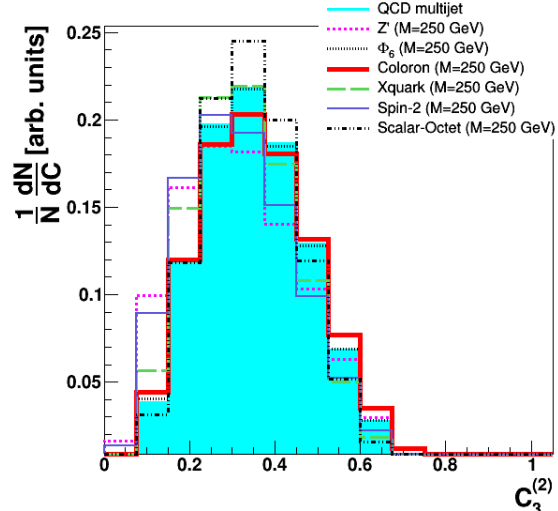


FIG. 3. The double ratio distributions for $C_3^{(2)}$ for the resonances and the multi-jet background.

background since, at low masses, the background is mostly gluonic in origin.

Further discrimination between resonances can be achieved by looking at the distribution for the higher moment correlator $C_3^{(\beta)}$ shown in Fig. 3. In contrast to $C_2^{(\beta)}$ we see that the peak of the distribution is shifted away from 0. This behavior can be better understood by considering the scenario where $X \rightarrow 1+2+3_{\text{soft}}+4_{\text{soft}}$. In this case, we assume that the transverse momentum distribution follows, $p_T^{j1} \simeq p_T^{j2} (= p_T) \gg (p_T^{j3}, p_T^{j4} = p_{T'})$ We can then approximate $C_3^{(\beta)}$ as (up to order $\varepsilon = \frac{p_{T'}}{p_T}$)

$$C_3^{(\beta)} \simeq \frac{[(R_{13}R_{14}R_{23}R_{24}R_{34})^\beta]}{[(R_{13}R_{23})^\beta + (R_{14}R_{24})^\beta]^2} + \mathcal{O}(\varepsilon)(5)$$

Thus the leading term is not proportional to ε , resulting in the peak that is shifted away from 0, and is determined by the relative opening angles. Similar to what we saw for the lower moment correlator, we find that the distribution of $C_3^{(2)}$ is shifted to larger val-

⁵ CMS [2] uses JEC in its search to discriminate between a Z' and background. The behavior of $C_2^{(2)}$, suggests that in addition to enhancing S/\sqrt{B} we can simultaneously use it to discriminate between resonances (S_8 being an exception).

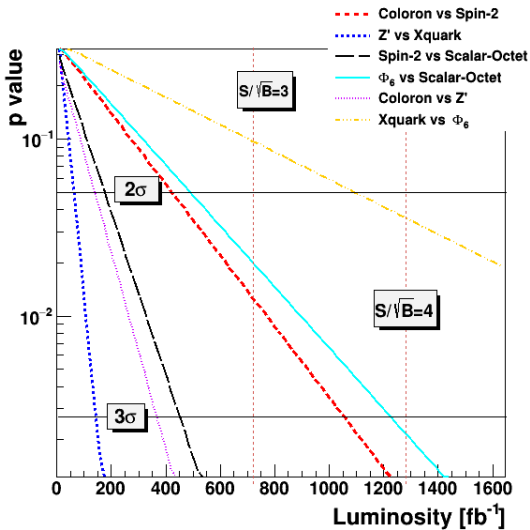


FIG. 4. The p -values testing hypothetical identities of various resonances as a function of luminosity. Horizontal lines indicate 2 and 3 σ exclusion of the alternate hypothesis. Vertical lines show where $S/\sqrt{B} = 3$ or 4.

ues depending on the dimensionality of the $SU(3)$ representation of the resonance as well as its decay products. The color singlet Z' decaying to a pair of quarks peaks closer to 0, whereas the distribution for the others, which either are octets or decay to gluons, is shifted away from 0.

An important point that should be noted finally is the dependence of the JEC on the exponent β . As $\beta \rightarrow 0$, the dependence on the relative angles vanishes, and the JEC double ratio approaches an (approximately) constant value away from 0. The exponent should therefore be viewed as a weighting factor that controls the size of the variation of the JEC. Note that we have not optimized β for maximal discrimination in this analysis. Another aspect that we have not investigated and have reserved for future study is the use of JECs (or other jet observables) on

unfiltered subjects to identify quark and gluonic jets. The ability to discern the decay products of these resonances would further enhance our ability to pinpoint the nature of the resonance.

In order to test the ability of JECs to characterize the nature of the resonance we perform a multi-variable likelihood analysis. We do not include $C_1^{(1)}$ in our likelihood function, since we are trying to test the information provided by radiation patterns and not kinematics. We therefore include only $C_2^{(2)}$ and $C_2^{(3)}$ in our likelihood function and test the ability of these two jet observables in differentiating the resonances. The result of our analysis is shown in Fig. 4. The horizontal dotted lines indicate where one can distinguish between various signal hypotheses at the 2 σ or 3 σ level; for example, one could tell a Z' from an excited quark at the 3 σ level with about 180 fb^{-1} of integrated luminosity. The vertical lines indicate the value S/\sqrt{B} provided by a given integrated luminosity; for instance, achieving $S/\sqrt{B} = 3$ for our resonances (since we assume the signal size is 25 fb^{-1}) would require 720 fb^{-1} of data. The figure shows that it is very easy to tell apart a coloron from a Z' , whereas the weakest discrimination is that between a spin-2 and a diquark.

In summary, we conclude that JECs are a powerful tool to both discover and identify new resonances at the LHC.

This material is based in part upon work supported by the National Science Foundation under Grant No. 1519045. We thank Wade Fisher and Joey Huston for useful discussions.

[1] Tech. Rep. ATLAS-CONF-2016-070, CERN, Geneva (2016), URL <http://cds.cern.ch/record/2206221>.

[2] A. M. Sirunyan et al. (CMS) (2017), 1705.10532.

[3] B. A. Dobrescu and F. Yu, Phys. Rev. **D88**, 035021 (2013), [Erratum: Phys. Rev. D90,no.7,079901(2014)], 1306.2629.

[4] R. S. Chivukula, A. G. Cohen, and E. H. Simmons, Phys. Lett. **B380**, 92 (1996), hep-ph/9603311.

[5] J. L. Hewett and T. G. Rizzo, Phys. Rept. **183**, 193 (1989).

[6] J. C. Pati and A. Salam, Phys. Rev. **D10**, 275 (1974), [Erratum: Phys. Rev. D11,703(1975)].

[7] N. Cabibbo, L. Maiani, and Y. Srivastava, Phys. Lett. **139B**, 459 (1984).

[8] U. Baur, I. Hinchliffe, and D. Zeppenfeld, Int. J. Mod. Phys. **A2**, 1285 (1987).

[9] C. T. Hill and E. H. Simmons, Phys. Rept. **381**, 235 (2003), [Erratum: Phys. Rept. 390,553(2004)], hep-ph/0203079.

[10] T. Han, J. D. Lykken, and R.-J. Zhang, Phys. Rev. **D59**, 105006 (1999), hep-ph/9811350.

[11] J. Thaler and K. Van Tilburg, JHEP **03**, 015 (2011), 1011.2268.

[12] J. M. Butterworth, A. R. Davison, M. Rubin, and G. P. Salam, Phys. Rev. Lett. **100**, 242001 (2008), 0802.2470.

[13] H.-n. Li, Z. Li, and C. P. Yuan, Phys. Rev. Lett. **107**, 152001 (2011), 1107.4535.

[14] J. Gallicchio and M. D. Schwartz, Phys. Rev. Lett. **105**, 022001 (2010), 1001.5027.

[15] A. Hook, M. Jankowiak, and J. G. Wacker, JHEP **04**, 007 (2012), 1102.1012.

[16] T. Han, I. Lewis, and Z. Liu, JHEP **12**, 085 (2010), 1010.4309.

[17] R. Sekhar Chivukula, P. Ittisamai, and E. H. Simmons, Phys. Rev. **D91**, 055021 (2015), 1406.2003.

[18] R. S. Chivukula, P. Ittisamai, K. Mohan, and E. H. Simmons, Phys. Rev. **D92**, 075020 (2015), 1507.06676.

[19] B. A. Dobrescu, K. Kong, and R. Mahbubani, Phys. Lett. **B670**, 119 (2008), 0709.2378.

[20] A. Alloul, N. D. Christensen, C. Degrande, C. Duhr, and B. Fuks, Comput. Phys. Commun. **185**, 2250 (2014), 1310.1921.

[21] J. Alwall, R. Frederix, S. Frixione, V. Hirschi, F. Maltoni, O. Mattelaer, H. S. Shao, T. Stelzer, P. Torrielli, and M. Zaro, JHEP **07**, 079 (2014), 1405.0301.

[22] T. Sjöstrand, S. Ask, J. R. Christiansen, R. Corke, N. Desai, P. Ilten, S. Mrenna, S. Prestel, C. O. Rasmussen, and P. Z. Skands, Comput. Phys. Commun. **191**, 159 (2015), 1410.3012.

[23] M. Cacciari, G. P. Salam, and G. Soyez, Eur. Phys. J. **C72**, 1896 (2012), 1111.6097.

[24] J. de Favereau, C. Delaere, P. Demin, A. Giannamico, V. Lemaître, A. Mertens, and M. Selvaggi (DELPHES 3), JHEP **02**, 057 (2014), 1307.6346.

[25] Y. L. Dokshitzer, G. D. Leder, S. Moretti, and B. R. Webber, JHEP **08**, 001 (1997), hep-ph/9707323.

[26] J. M. Campbell, R. K. Ellis, and W. T. Giele, Eur. Phys. J. **C75**, 246 (2015), 1503.06182.

[27] P. Nason, JHEP **11**, 040 (2004), hep-ph/0409146.

- [28] S. Frixione, P. Nason, and C. Oleari, JHEP **11**, 070 (2007), 0709.2092.
- [29] S. Alioli, P. Nason, C. Oleari, and E. Re, JHEP **06**, 043 (2010), 1002.2581.
- [30] M. L. Mangano, M. Moretti, F. Piccinini, R. Pittau, and A. D. Polosa, JHEP **07**, 001 (2003), hep-ph/0206293.
- [31] A. Banfi, G. P. Salam, and G. Zanderighi, JHEP **03**, 073 (2005), hep-ph/0407286.
- [32] M. Jankowiak and A. J. Larkoski, JHEP **06**, 057 (2011), 1104.1646.
- [33] A. J. Larkoski, G. P. Salam, and J. Thaler, JHEP **06**, 108 (2013), 1305.0007.